Chapter 5

First-principles Statistical Mechanics

DFT has proven to be a useful tool to investigate the electronic structure of materials. However, it provides only the total energy and is thus not directly applicable to situations at finite temperature [54]. Moreover, due to the unfortunate scaling of DFT, the accessible system sizes are limited. One would therefore often like to separate off large, but homogenous parts of the system and treat them only as reservoirs. For these cases, a suitable approach is first-principles statistical mechanics in which DFT is combined with concepts from thermodynamics or statistical mechanics. We will use such approaches in this work to account for the effect of realistic gas-phases with pressures of the order of atmospheres and elevated temperatures (*ab-initio thermodynamics* [55, 57, 58]), and to account for the effect of configurational entropy in the adsorbate ensemble (*ab-initio statistical mechanics*).

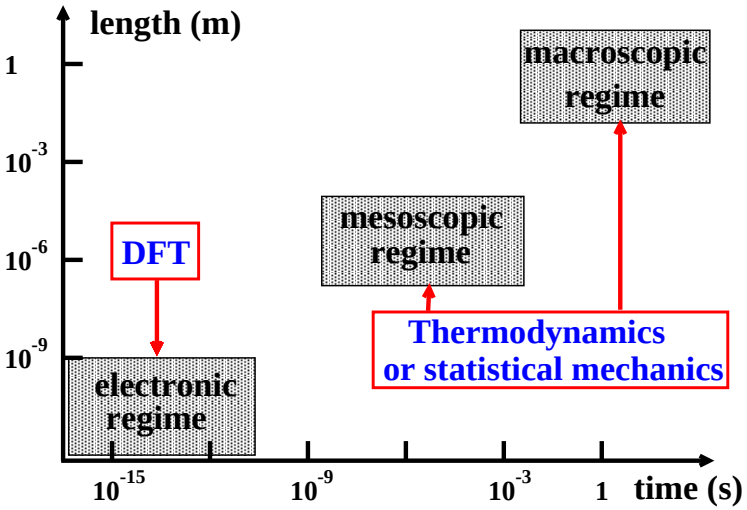

Figure 5.1: Schematic view of three regimes in the (length,time) space and methods used to simulate the corresponding regimes. The molecular processes occur in the *electronic regime*, whereas their statistical interplay develops in the *mesoscopic* and *macroscopic* regime.

5.1 Ab-initio Atomistic Thermodynamics

The total energies obtained by DFT correspond to the Helmholtz free energy at $T = 0$ K and neglecting the zero-point energy (ZPE). The effect of temperature and the ZPE can be drawn from calculating the potential energy surface (PES) at different atomic positions. A finite gas-phase pressure can be considered by assuming the surface to be in equilibrium with a reservoir exhibiting the appropriate thermodynamic potential.

If we correspondingly extend the surface energy definition of Eq. 4.8, we obtain the surface energy for oxygen adsorption at Pd surfaces in the (T, p) ensemble. Substituting the Gibbs free energy definition $G(T, p) = E - TS + pV$ into Eq. 4.7, we get

$$\gamma = \frac{1}{2A}(G_{\mathrm{O/Pd(slab)}}(T,p) - N_{\mathrm{Pd}}\mu_{\mathrm{Pd}} - N_{\mathrm{O}}\mu_{\mathrm{O}}) \quad , \tag{5.1}$$

where μ_{Pd} and μ_{O} are the chemical potentials of Pd and oxygen atoms, respectively. N_{Pd} and N_{O} are the number of Pd and O atoms in the adsorption system, respectively. The area A and the factor $1/2$ have the same meaning as in Eq. 4.8. Assuming the surface to be in equilibrium with the underlying metal bulk, μ_{Pd} is determined by the Pd bulk atoms. The vibrational entropic and pV terms in this bulk Gibbs free energy and the surface Gibbs free energy are rather similar. We therefore approximate the difference between these two quantities entering Eq. 5.1 by their leading total energy terms: $(G_{\mathrm{O/slab}}(T,p) - N_{\mathrm{Pd}}\mu_{\mathrm{Pd}}) \approx (E^{\mathrm{total}}_{\mathrm{O/slab}} - N_{\mathrm{Pd}}E^{\mathrm{total}}_{\mathrm{bulk}})$, and then arrive at,

$$\gamma = \frac{1}{2A}(E^{\mathrm{total}}_{\mathrm{O/Pd(slab)}} - N_{\mathrm{Pd}}E^{\mathrm{total}}_{\mathrm{bulk}} - N_{\mathrm{O}}\mu_{\mathrm{O}}) \quad . \tag{5.2}$$

Subtracting the surface energy of the clean surface, and supposing the number of Pd atoms in the O-covered slab and clean slab to not change, we get the Gibbs free energy of adsorption,

$$\Delta G(T,p) = \gamma - \gamma_{\mathrm{clean}} \approx -\frac{1}{2A}(E^{\mathrm{total}}_{\mathrm{O/Pd(slab)}} - E^{\mathrm{total}}_{\mathrm{Pd(slab)}} - N_{\mathrm{O}}\mu_{\mathrm{O}}) \quad . \tag{5.3}$$

Assuming the surface in equilibrium with the surrounding gas-phase the μ_{O} can be written as,

$$\mu_{\mathrm{O}}(T,p) = \frac{E^{\mathrm{total}}_{\mathrm{O_2(gas)}}}{2} + \Delta\mu_{\mathrm{O}} \quad . \tag{5.4}$$

Substituting into Eq. 5.3, and exploiting the definition for the binding energy we arrive at,

$$\begin{aligned} \Delta G(\Delta\mu_{\mathrm{O}}) &= -\frac{1}{2A}(E^{\mathrm{total}}_{\mathrm{O/Pd(slab)}} - E^{\mathrm{total}}_{\mathrm{Pd(slab)}} - N_{\mathrm{O}}(\frac{E^{\mathrm{total}}_{\mathrm{O_2(gas)}}}{2} + \Delta\mu_{\mathrm{O}})) \\ &= \frac{N_{\mathrm{O}}}{2A}(E_{\mathrm{b}} + \Delta\mu_{\mathrm{O}}) \quad . \end{aligned} \tag{5.5}$$

Table 5.1: $\Delta\mu_O(T, p^0)$ in the temperature range of interest to our study. The entropy and enthalpy changes used to obtain $\Delta\mu_O(T, p^0)$ are taken from [59] at p^0= 1 atm.

T	$\Delta\mu_O(T, p^0)$	T	$\Delta\mu_O(T, p^0)$
100 K	-0.08 eV	600 K	-0.61 eV
200 K	-0.17 eV	700 K	-0.73 eV
300 K	-0.27 eV	800 K	-0.85 eV
400 K	-0.38 eV	900 K	-0.98 eV
500 K	-0.50 eV	1000 K	-1.10 eV

The chemical potential of an oxygen atom in an ideal gas, $\Delta\mu_O(T, p)$, can be obtained using [55]

$$\Delta\mu_O(T, p) = \Delta\mu_O(T, p^0) + \frac{1}{2}k_B T ln(\frac{p_{O_2}}{p^0}) \quad , \tag{5.6}$$

where p^0= 1 atm, and $\Delta\mu_O(T, p^0)$ can be found in thermochemical tables [59]. We list some values for $\Delta\mu_O(T, p^0)$ of interest to our work in Table 5.1.

Eq. 5.5 can be used in a most straight forward way to determine the most stable surface structure by comparing the stability of different adsorbate phases depending on the gas phase condition, $\Delta\mu_O(T, p)$, and using the surface energy of the corresponding clean slab as reference energy. Fig. 5.2 illustrates this with the phase diagram of oxygen adsorption at the Pd(100) surface, which clearly shows three stable regions: The clean Pd(100) surface, as well as a $p(2\times2)$ and a $c(2\times2)$ adsorbate phase, which will be explained in more detail below [87–90, 92, 93].

5.2 Ab-initio Statistical Mechanics

In the above described formulation, the atomistic thermodynamics approach enables a first consideration of a surrounding environment. It is, however, restricted in its predictive character to those structures that are included in the comparison, *i.e.* it cannot predict unanticipated stable structures. The neglect of the surface configurational entropy furthermore limits its use for elevated temperature, *e.g.* order-disorder transitions in the adsorbate ensemble cannot be treated. In order to overcome these shortcomings, we use the first-principles Lattice Gas Hamiltonian (FP-LGH) approach in combination with Monte Carlo (MC) simulations to investigate corresponding phenomena.

5.2.1 Canonical Monte Carlo (CMC) [61, 62]

If we first want to explicitly address temperature effects on a fixed adsorbate ensemble, the appropriate ensemble to study thermodynamically is the (NVT) ensemble with

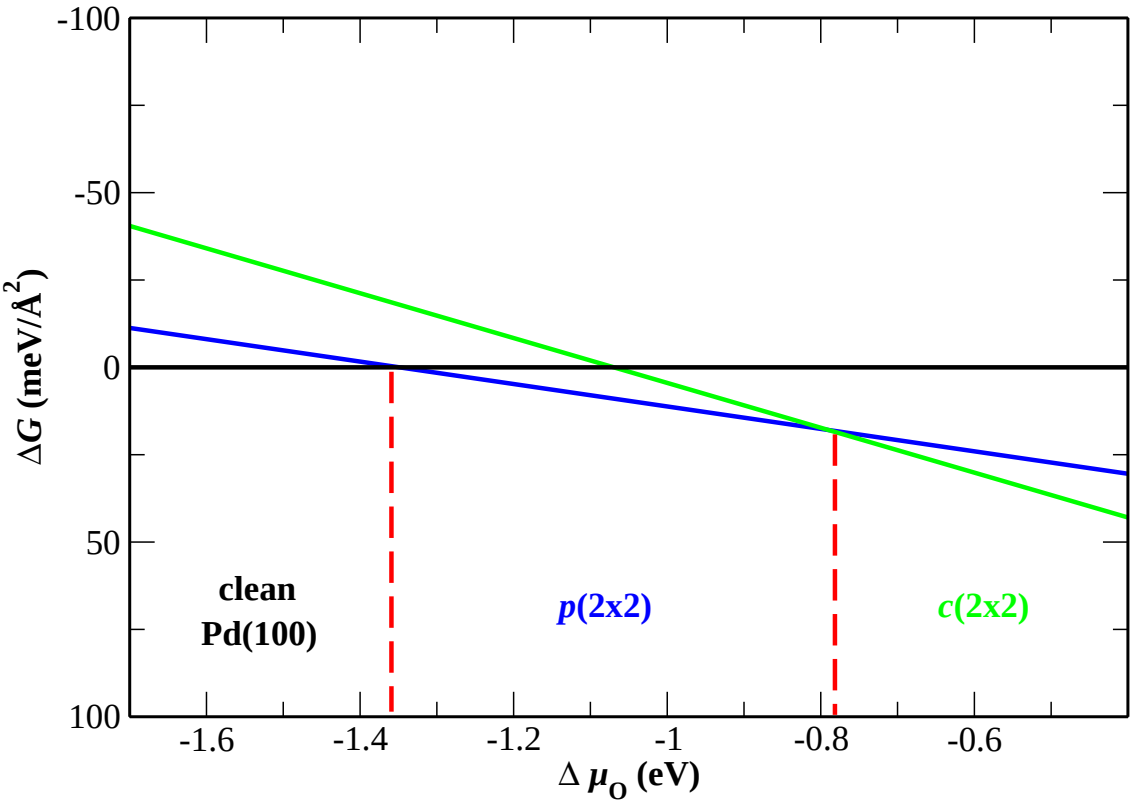

Figure 5.2: Phase diagram of on-surface oxygen atom adsorption at the Pd(100) surface. At low chemical potentials, the clean Pd(100) surface is the stablest structure $(-\infty, -1.35)$; with increasing chemical potential, oxygen atoms start to adsorb at the surface and build a $p(2 \times 2)$ configuration $(-1.35, -0.79)$; at further increased chemical potential, the $c(2 \times 2)$ configuration $(-0.79, +\infty)$ is coming out.

fixed number of particle N, fixed volume V, and fixed temperature T. The central quantity in this so-called canonical ensemble is the partition function,

$$Z = \sum_{\nu} e^{-E_\nu / k_B T} = \sum_{\nu} e^{-\beta E_\nu}, \quad (\beta = 1/k_B T) \quad . \tag{5.7}$$

where E_ν are the energies of the system states of interest and k_B is the Boltzmann constant, 1.38×10^{-23} J/K.

In this work, these system states of interest are any configuration of the adsorbates on the surface, ordered or disordered. For the moment we neglect vibrational contributions to the free energy, so that these system states are characterized by their total energy E_ν. We will thus intend to evaluate through Z the configurational entropy, and through $F = -kTlnZ$ the Helmholtz free energy. In more practical terms, we wish to evaluate the expectation value of any observable quantity Q in the corresponding (NVT) ensemble,

$$< Q >= \sum_{\nu} Q_\nu p_\nu = \frac{1}{Z} \sum_{\nu} Q_\nu e^{-\beta E_\nu} \quad , \tag{5.8}$$

where, Q_ν is the value of Q in state ν. The straight idea to calculate $< Q >$ is to calculate Z, $\sum_\nu Q_\nu e^{\beta E_\nu}$, and get $< Q >$. Unfortunately, it is tedious to calculate the integrand, and the scaling is (grid points)$^{\text{dimension}}$ for a grid-based techniques numerical integration. An efficient numerical approach is instead to resort to *Monte Carlo (MC)* simulations. The basic idea behind Monte Carlo simulations is to simulate the *random* thermal fluctuations of the system from state to state over the course of an experiment. In principle, one has to average the quantity of interest over all states ν of the system, and the real $< Q >$ is obtained when $\nu \to \infty$. However, this is only tractable for a very small system. For a large system, a much more efficient way would be to average only over the subset of system states, which have the largest contribution to the average quantity. The Monte Carlo technique thus works by choosing a subset of states at random from some probability distribution p_ν and thereby achieves an importance sampling. Hence, Eq. 5.8 is rewritten as,

$$Q_M = \frac{\sum_{i=1}^{M} Q_{\nu_i} p_{\nu_i}^{-1} e^{-\beta E_{\nu_i}}}{\sum_{i=1}^{M} p_{\nu_i}^{-1} e^{-\beta E_{\nu_i}}} \quad , \tag{5.9}$$

where, Q_M is an *estimator*. If M is large enough and nearly all important states are included, Q_M will approach the real $< Q >$. Particularly important is to realize that for Q_M to be a good estimator, one does not need the numerator and denominator in Eq. 5.9 to well approximate the infinite sums separately, but for a converged $< Q >$ only a well converged ratio of the two is necessary. Metropolis [64] devised an efficient Monte Carlo scheme to sample such a ratio. This so-called *Metropolis Algorithm* is described as follows:

1. If there are N particles in the system, and its total energy is E_1, we can give this configuration a probability distribution, $p_\nu = e^{-E_1\beta}$.

2. Randomly create a new configuration, and calculate the total energy of the new configuration, E_2. If E_2 is lower than E_1, accept the trial, and update the old configuration to the new one. Otherwise, accept the trial with a probability ($e^{-\beta\Delta E}$, $\Delta E = E_2 - E_1$). In practice this is realized by comparing $e^{-\beta\Delta E}$ with a random number (between 0 and 1). If $e^{-\beta\Delta E}$ is larger than the random number, accept the trial, and update the old configuration to the new one, otherwise reject the trial and continue with the old configuration.

3. Add the current configuration to the sums in Eq. 5.9.

4. Loop steps 1 to 3 steps until the estimator is converged to a given precision.

Since the system is allowed to visit any configuration in this scheme, it is clear that a large enough number of trials will enable the system to reach any phase space point of the system if the way to create new configuration is chosen appropriately. Hence, the method is *ergodic*.

5.2.2 Grand-Canonical Monte Carlo (GCMC)

In typical adsorption studies, the adsorbates do not only move at the surface, but also exchange with the gas-phase represented by a constant temperature and pressure. The appropriate ensemble to consider in this case is the grand-canonical ensemble (μVT), which means that chemical potential (μ), volume (V) and temperature (T) are fixed. The Metropolis scheme detailed in the previous sections can be readily extended to evaluate this ensemble as well. The corresponding grand-canonical Monte Carlo procedure is the following for a gas-phase reservoir characterized by the chemical potential $\Delta\mu(T,p)$ and again disregarding vibrational contributions to the free energy of the adsorbed particles for the time being:

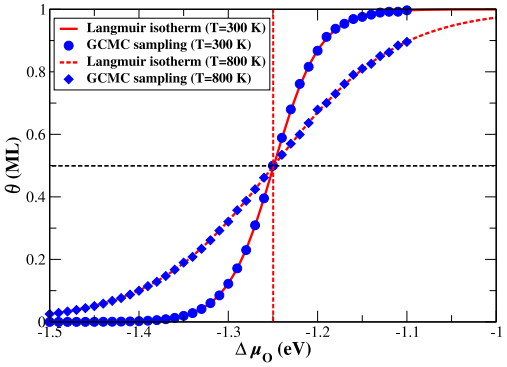

Figure 5.3: θ vs. $\Delta\mu$ from the Langmuir adsorption isotherm Eq. 5.10 (red solid line (300 K), red dashed line (800 K)) and GCMC simulation (blue dots (300 K), blue diamond (800 K)), respectively.

1. Prepare an initial configuration, containing N particles with total energy of E_1.

2. In the (μTV) ensemble, three cases can lead to new trial configurations: redistribution of the fixed number of particles at the surface, remove a particle from the surface, or add a particle to the surface. Each of the procedures has the same probability.

1). Removal: Randomly choose a particle, and move it from the surface to the reservoir. Then, calculate the total energy of this $(N-1)$ particle configuration, E_2, and the energy difference, $\Delta E = (E_2 + \Delta\mu) - E_1$. If $\Delta E < 0$, accept the removal. Otherwise, the removal should be accepted with a probability, $e^{-\beta\Delta E}$.

2). Addition: Randomly select an empty site, and add a particle from the reservoir to this site. The total energy of the new $(N+1)$ particle configuration, E_2, and the energy difference, $\Delta E = E_2 - (E_1 - \Delta\mu)$, are calculated. If $\Delta E < 0$, accept this addition. Otherwise, the addition should be accepted by a probability, $e^{-\beta\Delta E}$.

3). Diffusion: The same procedure as in CMC (see section 5.2.1).

3. Loop steps 1) to 3) until the observable Q_M is converged to a descried accuracy.

A simple numerical test to illustrate the GCMC approach is to evaluate the adsorption isotherm $(\Delta\mu, \theta)$, where θ is the coverage, for a lattice gas without lateral interactions. This model can also be evaluated analytically, leading to the Langmuir adsorption isotherm [76],

$$\theta = \frac{1}{1 + e^{\frac{E_0 - \Delta\mu}{k_B T}}} \quad , \tag{5.10}$$

where, θ is the coverage, E_0 is the binding energy of an adsorbated particle at the surface, and $\Delta\mu$ is the chemical potential difference to the particle in the gas-phase.

Fig. 5.3 shows a comparison of corresponding numerical GCMC results to the

analytical curve at $T = 300$ K and 800 K. The simulation cell was a square lattice of dimension (40×40). Based on the probabilities of removal and addition, in the low chemical potential ($\Delta\mu < E_0$) region, the probability to accept remove a particle from the surface is larger than adding a particle. This leads to $\theta < 0.5$ ML. On the contrary, when $\Delta\mu$ is larger than E_0, the probability to accept adding a particle to the surface is larger than removing a particle, and then the coverage is larger than 0.5 ML. At the point, $\Delta\mu = E_0$, the probabilities to accept removal and addition are equal and the equilibrium coverage is 0.5 ML. Furthermore, Fig. 5.3 shows that the curve at high T is more spread than at low T. This reflects the increased configurational entropy contribution at the higher temperature. Nevertheless, all curves must cross the (E_0, 0.5 ML) point.

5.2.3 First-principles Lattice-gas Hamiltonian (FP-LGH)

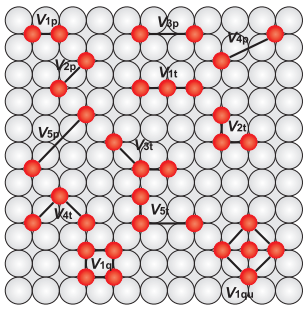

Figure 5.4: Schematic view of lateral interaction figures for adatoms at a fcc (100) surface.

While the importance sampling achieved by the described Metropolis schemes makes the evaluation of averaged properties in the (NVT) and (μVT) ensemble much more efficient, the total number of energy evaluations required is still untraceable for larger systems, if the total energies are provided directly from electronic structure calculations. In addition, due to the periodic boundary conditions the latter can only provide the energetics for ordered adsorbate configurations with rather small unit-cell sizes. For adsorption systems with site-specific adsorption this problem can be solved by resorting to a lattice model and expand the energy of any given configuration in terms of occupations in the lattice. This is the idea behind the *Lattice-Gas Hamiltonian* (LGH) [65−67] or *Cluster Expansion* (CE) approach, in which the total energy depends on an infinite expansion in terms of pair interactions, and many-body interactions, such as trio (three-body) interactions, quattro (four-body) interactions, and so on between well defined sites at the surface. As soon as the lateral interaction potentials are known, the total energy can be evaluated by a simple summation for any given configuration on the lattice, so that a manyfold evaluation of this Hamiltonian as required for MC simulations becomes readily possible.

Fig. 5.4 illustrates such a LGH model for adsorption of particles at a fcc (100) surface into the fourfold hollow sites. The LGH is then written (again neglecting vibrational contributions to the free energies for this time being):

$$E = \sum_{i=1}^{N} E_i^{\text{on-site}} n_i + \sum_{i \neq j} V_{\text{p}}(i,j) n_i n_j + \sum_{i \neq j \neq k} V_{\text{t}}(i,j,k) n_i n_j n_k + ... \qquad (5.11)$$

where, $E_i^{\text{on-site}}$ is the on-site energy, and V_{p} and V_{t} are pair and trio interactions, respectively. Formally, higher and higher order interaction terms (quattro, quinto, ...)

would follow in this infinite expansion. n_i is set as 1 or 0 according to site i being occupied or empty. In the LGH, the periodic boundary condition (Fig 5.5) should be considered in Eq. 5.11, which means that apart from the interactions between atoms in the simulation cell (green arrows), also the interactions with atoms in the neighboring image cells (blue arrows) should be considered.

As has been noted, the LGH expansion is in principle infinite including higher order interaction terms. In practice, the expansion must (and can) be truncated after a finite number of terms. One crucial objective to determine a reliable LGH is thus to identify which terms can be truncated. For a given truncated LGH the accuracy of the predicted total energies depends then on the accuracy of the considered lateral interactions, which is thus the second central objective to fit a reliable LGH. Traditionally, these parameters are adjusted in order to fit a variety of experimental data such as phase diagrams, heats of adsorption, or thermal desorption data. Although useful, such an approach is clearly not necessarily predictive in nature, nor the parameters unique, and may thus not capture the physics of the microscopic processes that are behind the best-fit adjusted effective parameters.

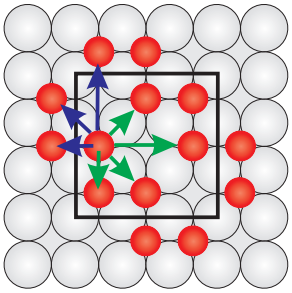

Figure 5.5: Schematic illustration of periodic image lateral interactions in the simulation cell. Green arrows are pair interactions in the simulation cell, while blue arrows are image pair interactions.

In recent years, algorithmic advances and increased computational power have made it possible to determine the lateral interactions alternatively from first-principles. Most notably, these are approaches that parameterize LGHs with DFT energetics. This is called *First-principles LGH* approach. In the FP-LGH, various ordered configurations at different coverages are calculated by DFT. For each configuration, the binding energy is expanded as a cluster expansion using Eq. 5.11. The on-site energies and lateral interactions can then be extracted by fitting to a sufficiently large number of such computed binding energies for different configurations. There are thus two crucial aspects that determine the reliability of this approach: One is which and how many lateral interactions play a role in determining accurate total energies. In other words, where should the CE be truncated? And the second one is which and how many DFT calculations are required to identify optimum lateral interactions. Obviously, the two questions are related to each other. In the next two sections, we are going to address these two intertwined topics.

5.2.4 Leave-one-out Cross-validation: Identify Optimum Lateral Figures

Suitable guidance for the question which lateral interactions should be considered in the truncated LGH expansion can be obtained by assessing the predictive character of the expansion. In other words, how well can the energetics of configurations that were

not used in the fitting of the lateral interactions be predicted. Due to the high cost of the underlying DFT calculations, it is not desirable to calculate a larger number of configurations as a test set with which this predictive character can be evaluated. Instead, one would want to use each computed configuration in the actual training set used to determine the lateral interactions. For such cases the predictive character can be assessed through cross-validation (CV) scores. The simplest one, the leave-one-out CV (LOO-CV) is defined as:

$$CV = \sqrt{\frac{1}{N}\sum_{i=1}^{N}(E_{\mathrm{b}}^{\mathrm{DFT}}(i) - E_{\mathrm{b}}^{\mathrm{LGH}}(i))^2} \quad . \tag{5.12}$$

where N is the number of calculated ordered configurations. $E_{\mathrm{b}}^{\mathrm{DFT}}(i)$ and $E_{\mathrm{b}}^{\mathrm{LGH}}(i)$ are the binding energies of the ith configuration by DFT calculation and evaluated from the LGH expression for this configuration, respectively. This method means that least-squares fitting (LSF) is applied on $(N-1)$ configurations to get the lateral interactions, and the remaining configuration is used to check the fitting data with an *expected error*. In more detail, the procedure of LOO-CV is: First, calculate N ordered configurations by DFT, and prepare a large pool of lateral interaction figures (like Fig. 5.4 or Fig. 6.1) according to the studied system. Second, randomly choose m lateral interaction figures from the pool. Instead of fitting them by least-square-fitting using ALL calculated configurations, leave the ith configuration out, use the rest $(N-1)$ configurations to fit the selected m figures by LSF, use the left out configuration to check the fitting data and get one expected error, $(E_{\mathrm{b}}^{\mathrm{DFT}}(i) - E_{\mathrm{b}}^{\mathrm{LGH}}(i))^2$. Then leave another configuration out, and fit the same m figures by the now remaining $(N-1)$ configurations by LSF, use the left out configuration to check the new fitting data and get another expected error. This loop is run until each configuration has been left out once and finally all expected errors are summed and averaged to produce the final CV score for the considered set of m lateral interactions. Then choose another group of m figures from the cluster pool, start anew, and get another CV score. This is equally done for all sets with $m-1$, $m+1$, $m-2$, $m+2$ ... *etc.* lateral interactions and finally the set of lateral interactions with the smallest CV score is identified as the optimum one.

5.2.5 Direct Enumeration: Validate the Set of DFT Input Structures

The LOO-CV identifies the optimum set of lateral interaction figures that minimizes the fitting errors for a given set of calculated configurations. This leaves the question, whether the configurations provide an ideal and sufficient set of input structures. One possibility to check on this is by assessing whether the LGH predicts the same set of ordered ground-state structures at T=0 K than the DFT input data. For our adsorption studies this is suitably evaluated through the formation energy, ΔE_f [69],

which is in general defined as an excess energy with respect to the equivalent amounts of pure constituents,

$$\Delta E_f = \frac{1}{N_\mathrm{t}}[E^\mathrm{total}_\mathrm{O/slab} - \theta E^\mathrm{total}_{(1\times1)-\mathrm{O/slab}} - (1-\theta)E^\mathrm{total}_\mathrm{slab}] \quad . \tag{5.13}$$

As in Eq. 4.9, $E^\mathrm{total}_\mathrm{O/slab}$ is the total energy for a specific adsorbate configuration with N_O O atoms per surface unit-cell (corresponding to a coverage $\Theta = N_\mathrm{O}/N_\mathrm{t}$ with N_t the number of sites per surface unit-cell), $E^\mathrm{total}_\mathrm{slab}$ is the total energy of the clean surface, and $E^\mathrm{total}_{(1\times1)-\mathrm{O/slab}}$ is the total energy of the full monolayer (1×1)-O configuration. With this definition, ΔE_f reflects the relative stability of a particular configuration with respect to phase separation into a fraction θ of the full monolayer configuration and a fraction $(1-\theta)$ of the clean surface, and we can relate it to the binding energy of the configuration by

$$\Delta E_f = \theta\left[E_{\mathrm{b,O/slab}} - E_{\mathrm{b},(1\times1)-\mathrm{O/Pd(100)}}\right] \quad . \tag{5.14}$$

Plotting the formation energy vs. coverage is very convenient to determine the *DFT ground state line* (or *convex hull*) [78]. As illustrated in Fig. 5.6, assume there are two stable configurations (θ_1,ΔE_{f1}) and (θ_2,ΔE_{f2}), and they define the DFT ground state line (dashed line in Fig. 5.6). Any formation energy (ΔE_{f0}) of a configuration at any coverage (θ_0) that lies on the dashed line can be easily derived by,

$$\Delta E_{f0} = \frac{\Delta E_{f2} - \Delta E_{f1}}{\theta_2 - \theta_1} \times \theta_0 \quad . \tag{5.15}$$

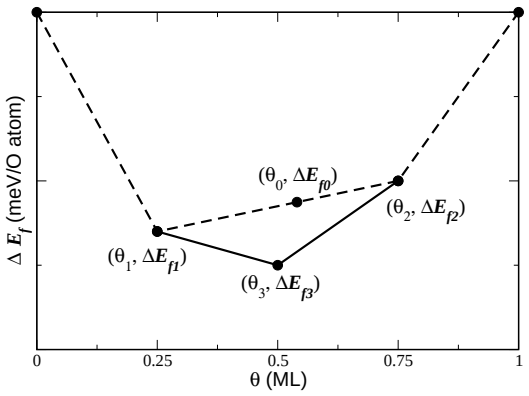

Figure 5.6: Schematic illustration of the idea behind a of convex hull and the ground line determined by formation energies.

Therefore, the ground state line divides the whole $(\theta, \Delta E_f)$ space into a unstable configuration region above the DFT ground line, and a stable configuration region below the line at least with respect to the existing DFT data (which here comprises only two configurations). If we now compute a third configuration (θ_3,ΔE_{f3}) that lies below the ground-state line a new stable structure is found and the convex hull/ground-state line must be redrawn (solid line in Fig. 5.6). For any newly computed configuration we can thus quickly assess whether it constitutes a stable structure at $T = 0$ K or not.

The LGH expansion should obviously predict the same stable structures as the DFT input data. An additional benefit is that with the LGH many more configurations within much larger unit-cells can be computed. By directly enumerating all such configurations within unit-cells with a certain maximum area, one can quickly check the consistency of the LGH with the DFT data. If there is LGH configuration that

leaks below the DFT ground-state line, the corresponding structure is obviously an important motif not yet included in the DFT input data set or it is an artifact of the present LGH expansion. In either case, this identifies a structure (or structural motif) that should be computed and included in the DFT input data set. For a refined LGH based on this new input data set, the procedure is repeated and again checked whether it predicts structures below the DFT ground-state line. This iterative scheme is done until DFT and LGH predict a consistent set of ground-state structures.

5.2.6 Two Properties to Monitor Phase Transitions: Ψ and C_V

Using a validated first-principles LGH in either canonical or grand-canonical MC simulations enables the study of critical phenomena at surfaces, like the order-disorder transition in the adsorbate ensemble. For this two central quantities that we will evaluate in the MC simulations are order parameters sensitive to the lateral periodicities at the surface (Ψ)[70–73] and the specify heat capacity (C_V).

Corresponding order parameters can be derived from Fourier theory for the periodicity of the ordered configuration of interest. Considering our two-dimensional periodic surfaces, the Fourier transformation should act on each dimension of the surface unit-cell. In this work, we are only interested in surface unit-cells with equal periodicity in both dimensions. We can correspondingly concentrate on a square Fourier matrix ($\mathbf{F}$) [68] written as:

$$\mathbf{F} = \begin{pmatrix} w^{0\cdot 0} & w^{0\cdot 1} & ... & w^{0\cdot(N_{\mathrm{FFT}}-1)} \\ w^{1\cdot 0} & w^{1\cdot 1} & ... & w^{1\cdot(N_{\mathrm{FFT}}-1)} \\ . & . & . & . \\ . & . & . & . \\ . & . & . & . \\ w^{(N_{\mathrm{FFT}}-1)\cdot 0} & w^{(N_{\mathrm{FFT}}-1)\cdot 1} & ... & w^{(N_{\mathrm{FFT}}-1)\cdot(N_{\mathrm{FFT}}-1)} \end{pmatrix} \quad , \tag{5.16}$$

where $w^{r\cdot c} = e^{-\frac{r\times c\times 2\pi i}{N_{\mathrm{FFT}}}}$: N_{FFT} indicates the periodicity in units of the surface unit-cell vector. In order to make a suitable transform according to our magnetization matrix $\mathbf{M}$ defined later, the Fourier transformed matrix ($\mathbf{R}$) is written as, [68]

$$\mathbf{R} = \mathbf{F} * (\mathbf{F} * \mathbf{M^T})^{\mathbf{T}} \quad . \tag{5.17}$$

where the superscript $\mathbf{T}$ denotes transposed the matrices transport without conjugation, which means that the operation only exchanges the rows and columns.

In our case the ordered arrangements of interest are $p(2\times 2)$ and $c(2\times 2)$ ordered adlayers as depicted in Fig. 5.7. In order to evaluate a suitable order parameter we apply the so-called renormalization group [70, 75], which divides the unit cell into several sub-lattices, a, b *etc* (Fig. 5.7). Supposing there are N_{sub} sub-lattices, we use M_a, M_b *etc* to indicate the total magnetization of the corresponding sub-lattices.

(The magnetization value of each site is 1 or -1 depending if the sites are occupied or empty.) The magnetization matrix of a configuration cell is thus expressed by a $(N_{\rm sub} \times N_{\rm sub})$ size matrix,

$$\mathbf{M} = \frac{1}{N_{\rm sub}} \begin{pmatrix} M_a & M_b & ... \\ ... & ... & ... \\ ... & ... & ... \end{pmatrix} \quad , \tag{5.18}$$

which has the same arrangement in its rows and columns as the unit-cell lattice at the surface. Correspondingly, the Fourier transform is written as a $(N_{\rm sub} \times N_{\rm sub})$ matrix as well. After transforming Eq. 5.17, the remaining non-zero elements in the matrix $\mathbf{R}$ compare to the frequencies, and are partly degenerate. Summing all these non-zero parts and normalizing so that the stable arrangement yields an order parameter of 1, we arrive at the final order parameter Ψ.

If we apply this general recipe to the $p(2 \times 2)$ ordered arrangement shown in the left panel of Fig. 5.7, we identify first $N_{\rm sub}$=4 sub-lattices, a, b, c and d. M_a, M_b, M_c and M_d are the corresponding magnetizations of the a, b, c and d sub-lattices in the simulation cell, respectively, and the magnetization matrix reads,

$$\mathbf{M}_{p(2\times2)} = \frac{1}{4} \begin{pmatrix} M_a & M_b & M_a & M_b \\ M_c & M_d & M_c & M_d \\ M_a & M_b & M_a & M_b \\ M_c & M_d & M_c & M_d \end{pmatrix} \quad , \tag{5.19}$$

Correspondingly, we can write its Fourier matrix as,

$$\mathbf{F}_{p(2\times2)} = \begin{pmatrix} 1 & 1 & 1 & 1 \\ 1 & e^{-\frac{\pi i}{2}} & e^{-\pi i} & e^{-\frac{3\pi i}{2}} \\ 1 & e^{-\pi i} & e^{-2\pi i} & e^{-\pi i} \\ 1 & e^{-\frac{3\pi i}{2}} & e^{-\pi i} & e^{-\frac{\pi i}{2}} \end{pmatrix}. \tag{5.20}$$

Substituting $\mathbf{M}_{p(2\times2)}$ and $\mathbf{F}_{p(2\times2)}$ into Eq. 5.17, we get,

$$\mathbf{R}_{p(2\times2)} = \begin{pmatrix} M_a + M_b + M_c + M_d & 0 & M_a - M_b + M_c - M_d & 0 \\ 0 & 0 & 0 & 0 \\ M_a + M_b - M_c - M_d & 0 & M_a - M_b - M_c + M_d & \\ 0 & 0 & 0 & 0 \end{pmatrix}. \tag{5.21}$$

Neglecting the constant part, $M_a + M_b + M_c + M_d = \theta \cdot N_{\rm t}$ ($N_{\rm t}$: the total number of sites in the simulation cell), the order parameter at 0.25 ML can be written as,

$$\Psi_{p(2\times2)} = \sqrt{(\Psi_1)^2 + (\Psi_2)^2 + (\Psi_3)^2} \quad , \tag{5.22}$$

where $\Psi_1 = M_a - M_b + M_c - M_d$, $\Psi_2 = M_a + M_b - M_c - M_d$, and $\Psi_3 = M_a - M_b - M_c + M_d$. Normalizing Eq. 5.22 to the most stable configuration, $p(2 \times 2)$ (left panel in Fig.

5.7), which gives $M_a = \frac{N_t}{4}$ and $M_b = M_c = M_d = -\frac{N_t}{4}$, we thus obtain $\Psi^{max}_{p(2\times2)} = \frac{3}{4N_t}$. Correspondingly, Eq. 5.22 is rewritten as,

$$\Psi_{p(2\times2)} = \frac{3}{4N_t}\sqrt{(\Psi_1)^2 + (\Psi_2)^2 + (\Psi_3)^2} \quad . \tag{5.23}$$

In the same spirit, for the $c(2 \times 2)$ ordered arrangement shown in the right panel in Fig. 5.7, we can identify 2 sub-lattices, N_{sub}=2, and the magnetization matrix is,

$$\mathbf{M}_{c(2\times2)} = \frac{1}{2}\begin{pmatrix} M_a & M_b \\ M_b & M_a \end{pmatrix} \quad , \tag{5.24}$$

Correspondingly, its Fourier matrix is,

$$\mathbf{F}_{c(2\times2)} = \begin{pmatrix} 1 & 1 \\ 1 & -1 \end{pmatrix}. \tag{5.25}$$

Substituting $\mathbf{M}_{c(2\times2)}$ and $\mathbf{F}_{c(2\times2)}$ into Eq. 5.17, we get,

$$\mathbf{R}_{c(2\times2)} = \begin{pmatrix} M_a + M_b & 0 \\ 0 & M_a - M_b \end{pmatrix}. \tag{5.26}$$

Neglecting the constant part, $M_a + M_b = \theta \cdot N_t$ (N_t: the total number of sites in the simulation cell), its order parameter is written as, $\Psi_{c(2\times2)} = \sqrt{(M_a - M_b)^2}$, where M_a and M_b indicate the total magnetization of a and b sub-lattices in the simulation cell, respectively. Normalizing this formula to the most stable $c(2 \times 2)$ configuration at this coverage, which gives $M_a = \frac{N_t}{2}$ and $M_b = -\frac{N_t}{2}$, we thus obtain $\Psi^{max}_{c(2\times2)} = \frac{1}{N_t}$ and arrive at the final order parameter at 0.5 ML,

$$\Psi_{c(2\times2)} = \frac{1}{N_t}\sqrt{(M_a - M_b)^2} \quad . \tag{5.27}$$

Such order parameters are perfect to determine the critical temperature for the order-disorder transition, if the periodicity of the ordered structure is known. Essentially, these order parameters are equivalent to the superstructure spot intensities in low-energy electron diffraction (LEED) experiments [74]. However, if the periodicity of the ordered structure is unknown, monitoring the specific heat capacity C_V is another suitable approach, which is instead sensitive to the mean squared fluctuations in energy [75]. This quantity is defined as,

$$\begin{aligned} C_V &= \frac{< E^2 > - < E >^2}{k_B T^2} \\ &= \frac{\frac{\sum_i^M E_i^2}{M} - (\frac{\sum_i^M E_i}{M})^2}{k_B T^2} \quad , \end{aligned} \tag{5.28}$$

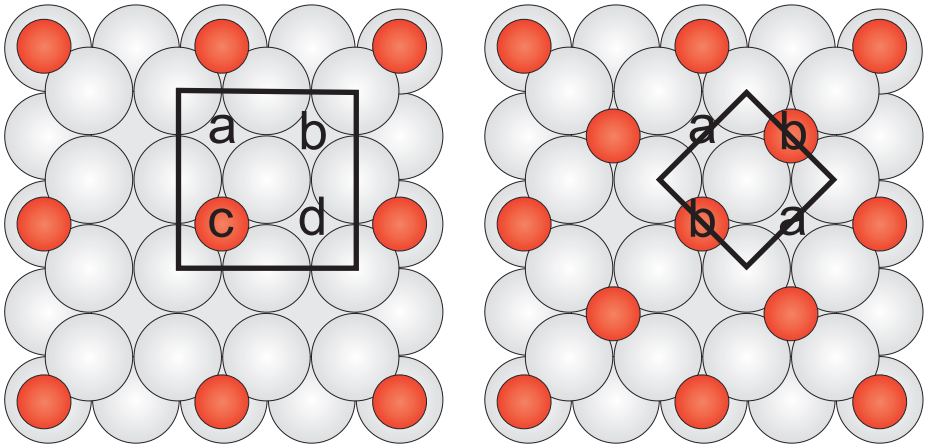

Figure 5.7: Schematic top view illustrating the division into sub-lattices for the $p(2 \times 2)$ (left panel) and $c(2 \times 2)$ structures (right panel) on a fcc (100) surface. There are 4 and 2 sub-lattices for the $p(2 \times 2)$ and $c(2 \times 2)$ configurations, respectively. a, b, c or d indicate the name of one kind of sub-lattice. (Large spheres Pd atoms, small spheres O adatoms)

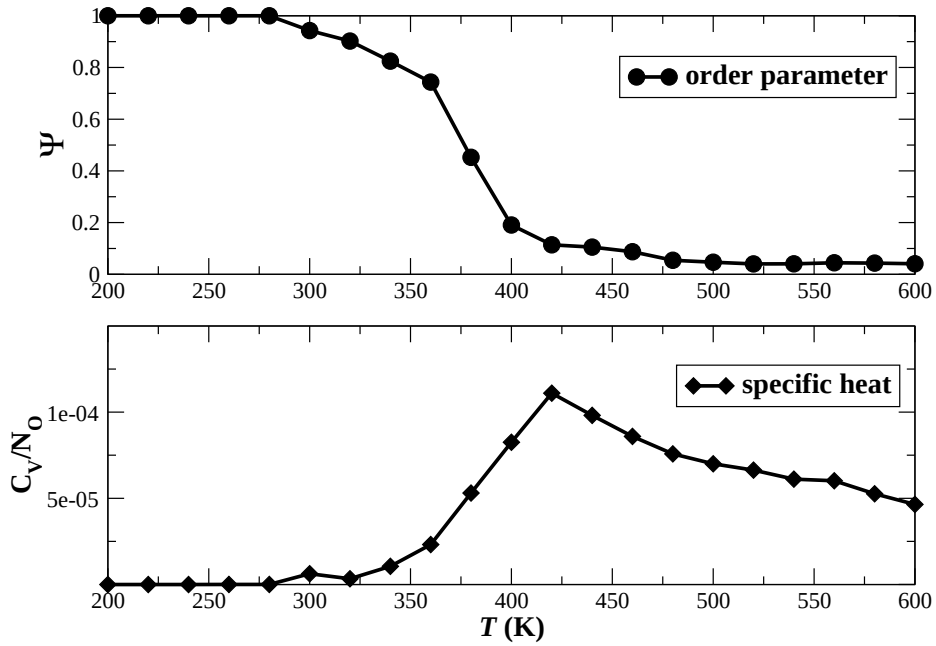

Figure 5.8: Illustration of how the order parameter Ψ (upper panel) and the specific heat C_V (lower panel) identify the order-disorder transition of a $p(2 \times 2)$ structure at a cubic (100) surface with $\theta = 0.25$ ML. As a toy model we consider a strongly repulsive first nearest neighbor pair interaction (-200 meV) and a smaller repulsive second nearest neighbor pair interaction (-50 meV) between adatoms adsorbed into the hollow sites of the (100) surface. Evaluating Ψ and C_V over 10^8 MC steps and in a (60×60) simulation cell, both properties yield a critical temperature (taken from the inflection point for Ψ and from the peak for C_V) that is identical to within 40 K.

where, $< E >$ and $< E^2 >$ are the average energy and the mean squared energy, respectively, and M is the number of MC steps. Fig. 5.8 illustrates an example of how Ψ and C_V identify the order-disorder transition.

Furthermore, for a (100) surface including one (111) step, in order to study the (111) step effects on the mesoscopic adsorption properties at the (100) surface, we need to define a property that is sensitive to the local environment. For this we employ the specific heat per atom resolved for each row parallel to the (111) step, C_V^{row}. Since the number of atoms in each row is then no longer constant during the MC simulation we thus rewrite Eq. 5.28 as

$$C_V^{\mathrm{row}_j} = \frac{1}{kT^2}\left[\frac{\sum_{i=1}^{M}\left(\frac{E_i^{\mathrm{row}_j}}{\sqrt{N_i^{\mathrm{row}_j}}}\right)^2}{M} - \left(\frac{\sum_{i=1}^{M}\frac{E_i^{\mathrm{row}_j}}{\sqrt{N_i^{\mathrm{row}_j}}}}{M}\right)^2\right] \quad , \tag{5.29}$$

where, $N_i^{\mathrm{row}_j}$ and $E_i^{\mathrm{row}_j}$ are the number of atoms and the total energy in the jth row at the ith MC step. (See the test for O-Pd(100) in Appendix D.)